32

Prandtl Number Effect on Heat Transfer Degradation in MHD Turbulent Shear Flows by Means of High-Resolution DNS

Yoshinobu Yamamoto and Tomoaki Kunugi
Department of Nuclear Engineering, Kyoto University
Japan

1. Introduction

Estimation of the heat transfer degradation effected by Magneto-Hydro-Dynamics (MHD) forces is one of the key issues of the fusion reactor designs utilized molten salt coolant. FLiBe which is the molten salt mixture of LiF and BeF, is one of the coolant candidates in the first wall and blanket of the fusion reactors, and has several advantages which are little MHD pressure loss, good chemical stability, less solubility of tritium and so on. In contrast, heat transfer degradation for the high Prandtl number, (Pr=ν/α, Prandtl number, ν is the kinetic viscosity, α is the thermal diffusivity) characteristics caused by the low thermal diffusivity and high viscosity (Sagara et al, 1995), was one of the issues of concern.
MHD turbulent wall-bounded flows have been investigated extensively by both experimental and numerical studies (Blum, 1967, Reed & Lykoudis, 1978, Simomura, 1991, Lee & Choi, 2001, Satake et al., 2006, Boeck et al, 2007, etc.) and much important information such as the drag reduction, the turbulent modulation, similarity of velocity profile, and heat transfer have been obtained.
On the other hands, MHD turbulent heat transfer in a high-Pr fluid has not been understood well. The previous experimental and direct numerical simulation (DNS) studies still have conducted for Prandtl number up to Pr=5.7. Therefore, the knowledge of the MHD heat transfer on higher-Pr fluids such as FLiBe (Pr=20–40), is highly demanded to verify and validate the MHD turbulent heat transfer models for the fusion reactor designs.
The objective of this study is to perform a direct numerical simulation of MHD turbulent channel flow for Prandtl number up to Pr=25, where all essential scales of turbulence are resolved. In this study, we report that the MHD turbulent heat transfer characteristics in Pr=25 for the first time and discuss that the MHD pressure loss and heat transfer degradation under the wide-range Pr conditions. The obtained database is of considerable value for the quantitative and qualitative studies of the MHD turbulent heat transfer models for the blanket design of a fusion reactor.

2. Target flow field and flow condition

The flow geometry and the coordinate system are shown in figure 1. The target flow fields are the 2-D fully-developed turbulent channel flows imposed wall-normal magnetic field

and the streamwise and spanwise computational periods (L_x and L_z) are chosen to be $8h$ and $4h$, where h (=L_y/2) denotes channel half height.

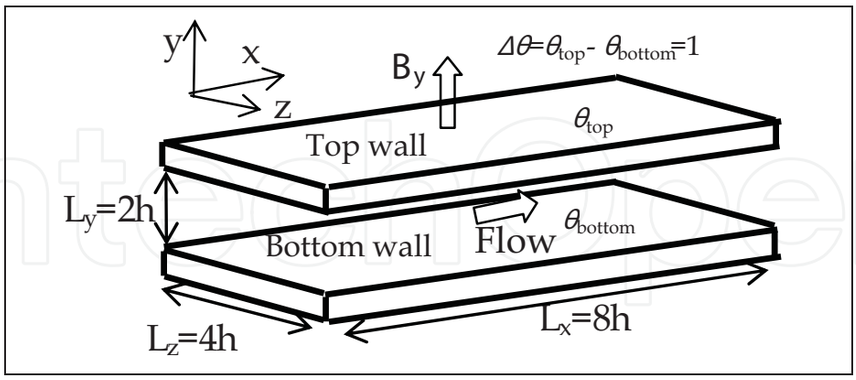

Fig. 1. Flow geometry and coordinate system

	Re_τ	Ha	Pr	Grid number N_x,N_y,N_z (M_x,N_y,M_z)	Resolution $\Delta x^+,\Delta y^+,\Delta z^+$ (temperature)
CASE1 (Lithium)	150	0,8,10,12	0.025	72,182,72	16,7,0.25-2.0,8.3
CASE2 (KOH)		0,6,8,10,12	5.7		
CASE2′ (fine grid)		0	5.0	432,182,216	2.8,0.25-2.0,2.8
CASE3 (FLiBe)		0,8,10,12	25.0	72,370,72 (320,370,160)	16.7,0.05-1.0,8.3 (3.8,0.05-1.0,3.8)
CASE3′ (fine grid)		0	25.0	648,370,324	1.9,0.05-1.0,1.9

Table 1. Numerical condition

Duo to the limitation of our utilizable computational resources, turbulent Reynolds number ($Re_\tau=u_\tau h/\nu$, u_τ: friction velocity) was limited to 150, and three thermal properties of the Lithium (Pr=0.025), KOH solution (Pr=5.7), and FLiBe (Pr=25) were covered. The KOH solution was used as the FLiBe simulant fluid in the previous experimental study (Yokomine et al., 2007) and the Lithium is a typical liquid metal coolant in a blanket of fusion reactors. To maintain the fully-developed turbulent status, Hartman number ($Ha=B_y 2h(\sigma/\rho\nu)^{1/2}$, B_y: wall-normal magnetic flux density, σ: electrical conductivity, ρ: density) was also limited around 12 in Re_τ=150 (Lee & Choi, 2001, Yamamoto et al., 2008).
Numerical conditions are tableted in Table 1. Here, $N_x(\Delta x)$,$N_y(\Delta y)$, and $N_z(\Delta z)$ are the grid numbers (resolutions) in the streamwise, vertical, and spanwise directions, respectively. The super-script + denotes the nondimensional quantities normalized by the friction velocity, friction temperature and the kinematic viscosity. M_x and M_z are also the grid numbers in a horizontal direction temperature as mentioned 3.2, in case of adapting a different grid resolution for the flow and for the temperature field. In a wall-normal direction, the grid resolution resolved the Batchelor scale is ensured for all cases.

3. Numerical procedures

3.1 Governing equation and boundary condition

Governing equations of the present DNS are the continuity equation (1), the momentum equations (2) with the electric field described using the electrical potential approach (Simomura, 1991), Poisson equation (3) of the electrical potential, and the energy equation (4).

$$\frac{\partial u_i^*}{\partial x_i} = 0, \tag{1}$$

$$\frac{\partial u_i^*}{\partial t} + \frac{\partial u_i^* u_j^*}{\partial x_j} = \frac{F_i}{\rho}\delta_{i1} - \frac{\partial}{\partial x_i}\left(\frac{p^*}{\rho}\right) + \nu\frac{\partial^2 u_i^*}{\partial x_j \partial x_j} + \frac{\sigma}{\rho}B_{ijk}\left(-\frac{\partial \varphi^*}{\partial x_j} + \varepsilon_{jlm}u_l^* B_m\right)B_k, \tag{2}$$

$$\frac{\partial^2 \phi^*}{\partial x_i \partial x_i} = \frac{\partial}{\partial x_i}\left(\varepsilon_{ijk}u_j^* B_k\right), \tag{3}$$

$$\frac{\partial \theta^*}{\partial t} + \frac{\partial \theta^* u_j^*}{\partial x_j} = \alpha\frac{\partial^2 \theta^*}{\partial x_j \partial x_j}. \tag{4}$$

Here u_i and x_i are the streamwise (i=1), the vertical (i=2) and the spanwise (i=3) velocity and direction, respectively. t is time, F_i is the i-th competent mean pressure gradient, p is the pressure, ϕ is the electric potential, B_i=(0, B_y,0) is the Magnetic flux density, and θ is the temperature. Super script * denotes instantaneous value and δ_{ij}, ε_{ijk} (i,j,k=1-3) is the Kronecker delta and the Levi-Civita symbol, respectively.

Non-slip and periodic conditions are imposed for the boundary conditions of velocities and the constant temperature at top and bottom boundaries ($\theta_{top} > \theta_{bottom}$, θ_{top}: top wall temperature, θ_{bottom}: bottom wall temperature), and the periodic conditions are imposed for the temperature field. In this study, temperature transport is treated as a passive scalar.

The non-conducting conditions of the electric potential are applied to all walls and the periodic condition imposed on the horizontal directions. Total electric current in the spanwise flow domain is kept zero.

3.2 Numerical procedures

A hybrid Fourier spectral and the second-order central differencing method (Yamamoto et al, 2009) is used for the computations. The spectral method is used to compute the spatial discretization in the stream (x) and spanwise (z) directions. Nonlinear terms are computed with 1.5 times finer grids in horizontal (x and z) directions to remove the aliasing errors (Padding method). The derivative in the wall normal (y) direction is computed by a second-order finite difference scheme at the staggered grid arrangement (Satake et al, 2006). Time integration methods of the governing equations are the 3rd-order Runge-Kutta scheme for the convection terms, the Crank-Nicolson scheme for the viscous terms and the Euler Implicit scheme for the pressure terms, respectively. The Helmholtz equation for the viscous (diffusion) terms and the Poisson equations of the pressure and the electrical potential are solved by a Tri-Diagonal Matrix Algorithm, TDMA in Fourier space.

In DNS of the flow field, the Kolmogorov length scale has to be resolved. On the other hands, the length scales of the high-Pr temperature field are smaller than the smallest length scales of the velocity fields (Batchelor, 1959). To reduce the numerical costs in DNS of the

high-Pr fluids, a different number of grid resolutions in the horizontal direction for velocity and temperature fields is adapted. In computing the temperature convection terms in (4) pseudo-spectrally, the grid points of velocities were expanded to the same grid points of the high-Pr temperature, as follow,

$$\Phi(k_x,y,k_z)=\begin{cases}\Phi(k_x,y,k_z) & |k_x|\le \pi N_x / L_x, |k_z|\le \pi N_z / L_z \\ 0 \text{ otherwise} & \end{cases}, |k_x|\le \pi M_x / L_x, |k_z|\le \pi M_z / L_z. \quad (5)$$

Here, Φ denotes the velocities in Fourier space, k_x and k_z are the wavenumbers in the streamwise and spanwise directions, respectively. The phase-shift method (Patterson & Orszag, 1971) is used to remove the aliasing errors derived from the temperature convection terms. As a consequence, the grid size corresponded to the Batchelor length scale is retained for Pr=25.

Present DNS were calculated by using the T2K Open Supercomputer at Kyoto University. Elapsed time per one time step was about 1.2 [s] when using 8nodes (128cores) in CASE3.

4. Validation of present DNS

At the beginning of this study, we demonstrate the adequacy of the present DNS.

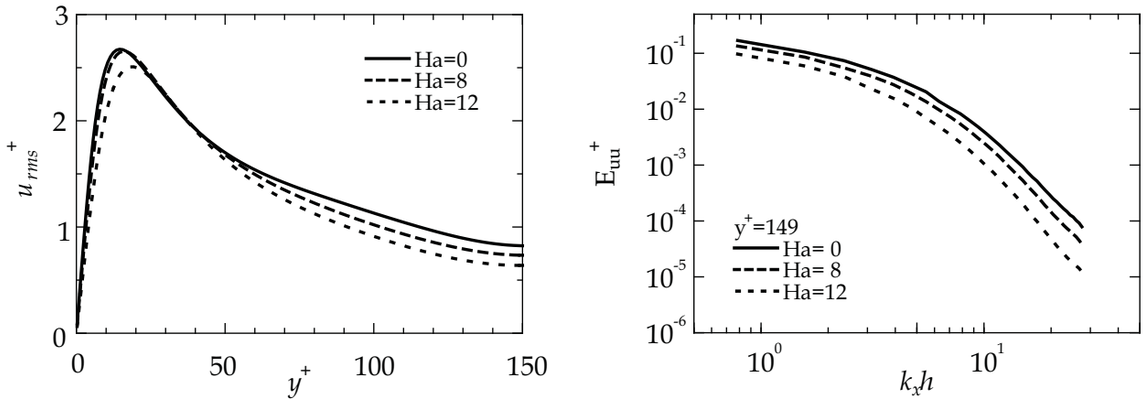

(a) Streamwise turbulent intensity, (b) Streamwise energy spectra,

Fig. 2. MHD suppression effects on turbulence

Figures 2 shows the turbulent intensities and the streamwise energy spectra at the channel center in Ha=0, 8, and 12. As well as the previous study (Lee & Choi, 2001), turbulent intensity was suppressed with increase of Ha as shown in Fig. 2-(a). Figure 2-(b) gives evidence that turbulent suppression effects can be remarkable in the high wave-numbers turbulence. It is clear that the effects of the grid dependency would be the biggest in Ha=0. Therefore, the convergences of the grid tendency were investigated in Ha=0, by using the DNS data fully-resolved the Batchelor length scale for Pr=5 or 25 in Ha=0 as tabled CASE2′ and CASE3′ in Table 1.

4.1 Medium high-Pr case

According to Na & Hanratty, 2000, the use of a higher resolution in horizontal direction does not produce significant changes to the first-order statistics from Pr=1 to 10. In this

study, we investigated the grid dependency effects on the higher-order statistics such as the energy dissipation (=ε) and temperature energy dissipation (=ε_θ).

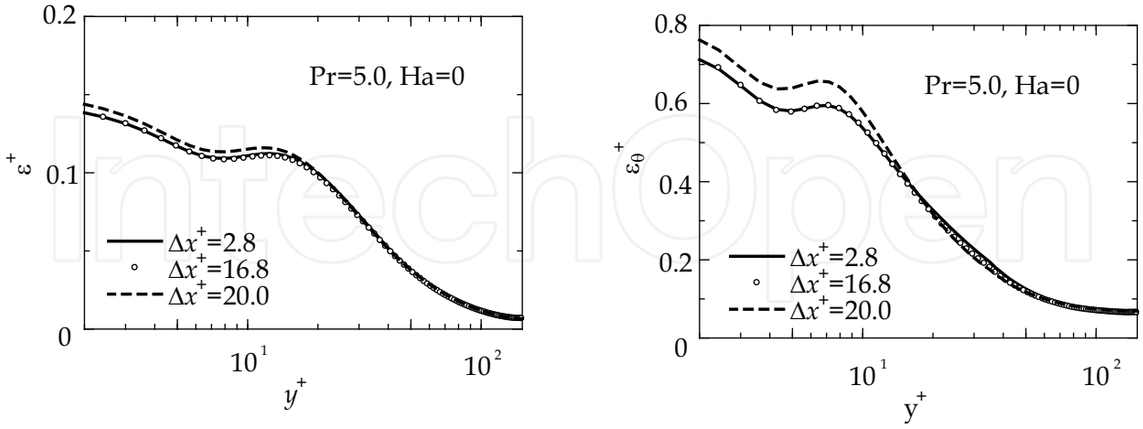

(a)energy dissipation, (b) temperature energy dissipation,

Fig. 3. Grid dependency on high-order statistics in medium high-Pr fluid

Figures 3 show the energy dissipation and temperature energy dissipation for Pr=5 with change of the horizontal resolutions. The required horizontal resolution for the reproductively of the energy dissipation and temperature dissipation, was estimated as Δx^+=16.7, and Δz^+=8.3 in this medium high-Pr fluid.

4.2 High-Pr case

For Pr=25, DNS in Re_τ=180 were conducted by means of a hierarchical algorithm in which only the scalar fields were solved on the grid dictated by the Batchelor scale (Schwertfirm &Manhart, 2007). However, the validation by using the different resolution for flow and high-Pr temperature field has not been reviewed yet. In this study, the adequacy of DNS by using a different resolution for flow and high-Pr temperature field is verified compared with DNS data fully-resolved the Batchelor length scale in the same grid size for flow and temperature.

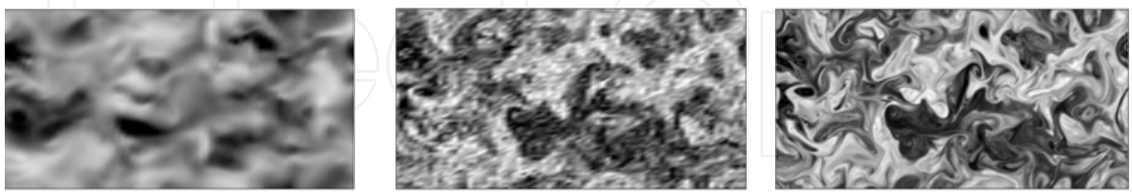

(a) (b) (c)

Fig. 4. Flow visualization, CASE3, Ha=0, Pr=25, y^+=149. (a) streamwise turbulent velocity, -2 (black) < u^+ < 2.0 (white), (b) turbulent temperature (coarse grid), -0.15 (black) < $\theta/\Delta\theta$ <0.15 (white) (c) turbulent temperature (fine grid), -0.15(black)<$\theta/\Delta\theta$<0.15 (white)

Figure 4 shows the flow visualization in results of Ha=0, Pr=25. In this case, 72x72 grids for flow (in Fig.4-(a)), 72x72 grids for the temperature filed (in Fig.4-(b)) and 320x160 grids for the temperature field (in Fig.4-(c)), were used in horizontal directions, respectively. Despites

of the high wave-number flow fluctuations, the high wave- number temperature fluctuation can be computed as shown in Fig.4-(c).

Figure 5-(a) shows the temperature energy dissipation for Pr=25 with change of the horizontal resolutions. The required horizontal resolution for the reproductively of the temperature dissipation, was estimated as Δx^+=8.3, and Δz^+=4.2. This grid resolution is equivalent to twice as high for Pr=5; it is proportional to square root of the Pr ratio (=$(25/5)^{1/2}$). The effects of using the different resolution for flow and temperature cannot be found even in the temperature energy dissipation.

Figure 5-(b) shows the streamwise energy spectra near channel center for Pr=25. Compared with CASE3 and CASE3', there is ninefold grid resolution in flow, but the variance of the spectra profile cannot be observed in this high-Pr temperature field. This indicates that the high wave-number velocity fluctuations less than the Kolmogorov scale can be ignored in a high-Pr passive scalar transport. As a consequence, we verify the adequacy of DNS by using the different resolution for flow and high-Pr temperature field and numerical cost in DNS of high-Pr fluids can be substantially reduced.

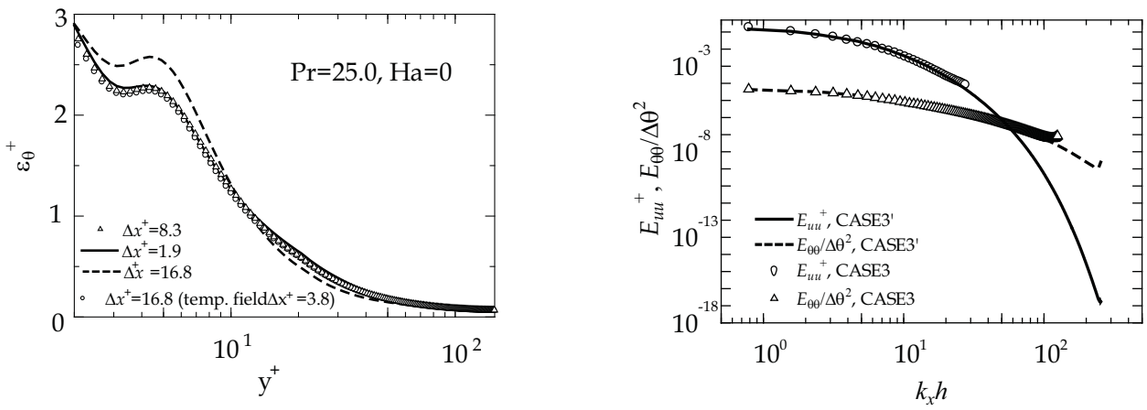

(a) (b)

Fig. 5. Grid dependency and validation of different grid resolution for flow and high-Pr temperature field. (a) Temperature dissipation, (b) Streamwise energy spectra, streamwise velocity and temperature

5. MHD pressure loss and heat transfer

In this study, the friction drag confident (Cf) and Nusselt number (Nu) at the wall were expressed by

$$Cf=2u_\tau^2/U_b^2, \tag{6}$$

$$Nu=2h(d\Theta/dy)_{wall}/\Delta\theta. \tag{7}$$

Here, U_b and $(d\Theta/dy)_{wall}$ denotes the bulk mean velocity and mean temperature gradient at the wall.

Figure 6-(a) shows the friction drag coefficient as a function of the interaction parameter N (=Ha^2/Re_b, Re_b: Bulk Reynolds number=$U_b 2h/\nu$), where the friction drag coefficients were normalized by that in Ha=0. The friction drag coefficients were monotonically decreased

with increase of Ha; MHD pressure loss is less than the turbulent drag reduction effected by MHD. Therefore, all MHD cases of this study might be considered in a turbulent-laminar transition status. We need the DNS data in more higher Re to discuss the general relationships between MHD pressure loss and MHD turbulent drag reduction in turbulent condition.

Figure 6-(b) shows the Nusselt number as a function of N, where the Nusselt number were also normalized by that in Ha=0. Maximum heat transfer degradation in the low-Pr fluid was no more than 5% of the non-MHD condition. The usability of a low-Pr fluid was no doubt about heat transfer, however, Ha of Lithium was 700 times as large as one of FLiBe in the same Reynolds number (Re) and magnetic flux density (B_y) conditions.

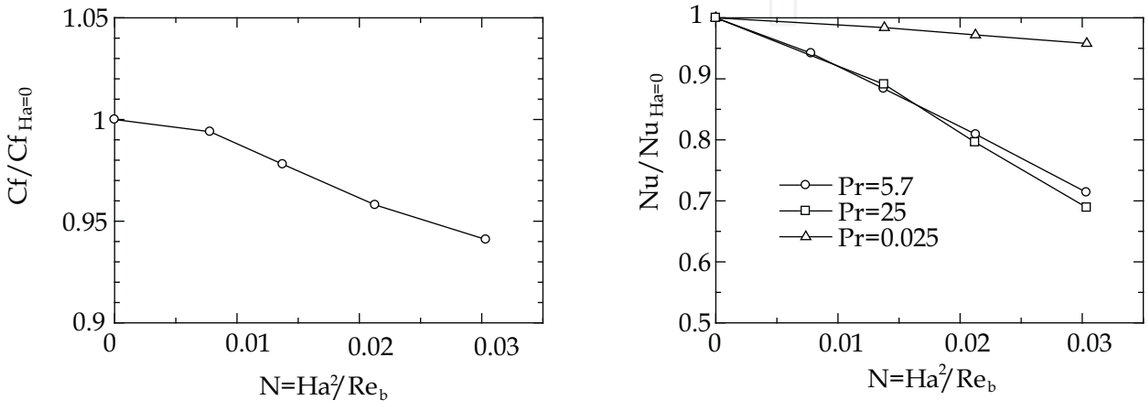

(a) friction drag coefficient, (b) Nusselt number,

Fig. 6. Friction drag coefficient and Nusselt number as a function N

On the other hands, heat transfer degradation in the high-Pr fluids (Pr=5.7 and 25) reached up to 30% without depending on Pr. This indicated that similarity of heat transfer degradation in high-Pr MHD flows might be existed.

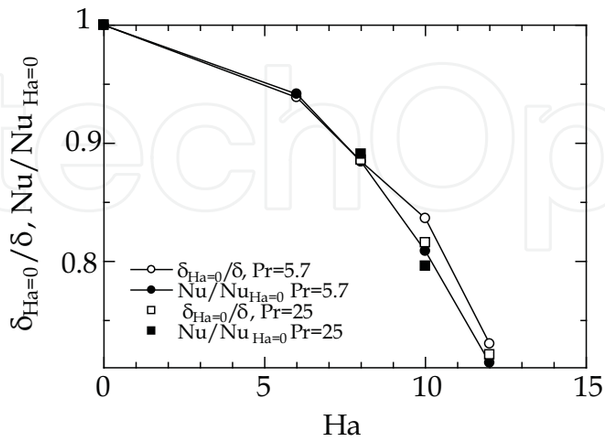

Fig. 7. Thermal viscosity thickness and Nusselt number as a function N

Figure 7 shows the thermal viscosity thickness (δ) and Nusselt number as a function of Ha in the high-Pr fluids, where thermal viscosity thickness was defined as

$$\delta = y^+ \text{ at } \Theta^+ = 0.99 \mathrm{Pr} y^+. \quad (8)$$

Thermal viscosity thickness was normalized by those in Ha=0. Heat transfer degradation was strongly correlated with change of the thermal viscosity thickness without depending on Pr.

6. Turbulence statistics

Figure 8 shows the profiles of temperature turbulent intensities for Pr=5.7 and 25. With increase of Ha, the peak position of turbulent intensity was shifted to the channel center side and the scale of it was decreased in both cases. In either case, the peak position was located below the wall-normal height y^+=15; thermal boundary layers for Pr=5.7 and 25 were thinner than the velocity boundary layer in the present MHD conditions.

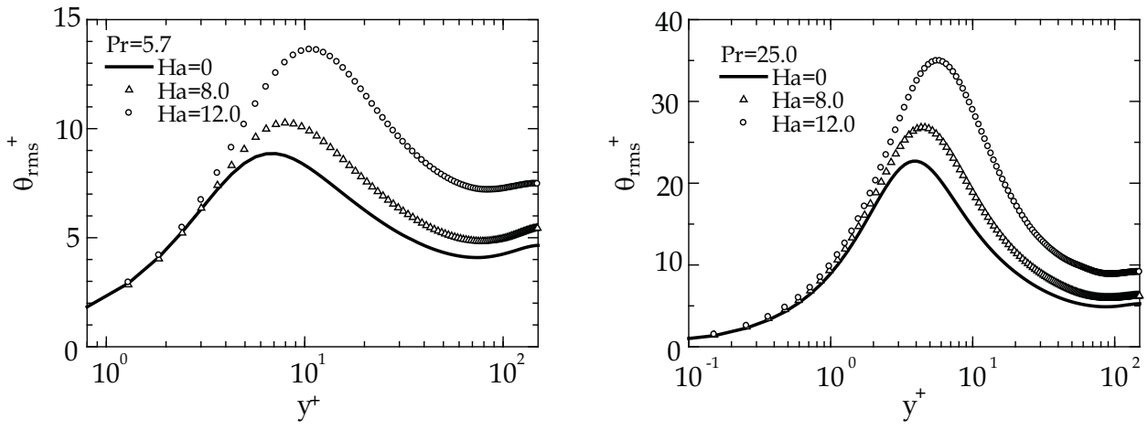

(a) Pr=5.7, (b) Pr=25,

Fig. 8. Turbulent temperature profiles

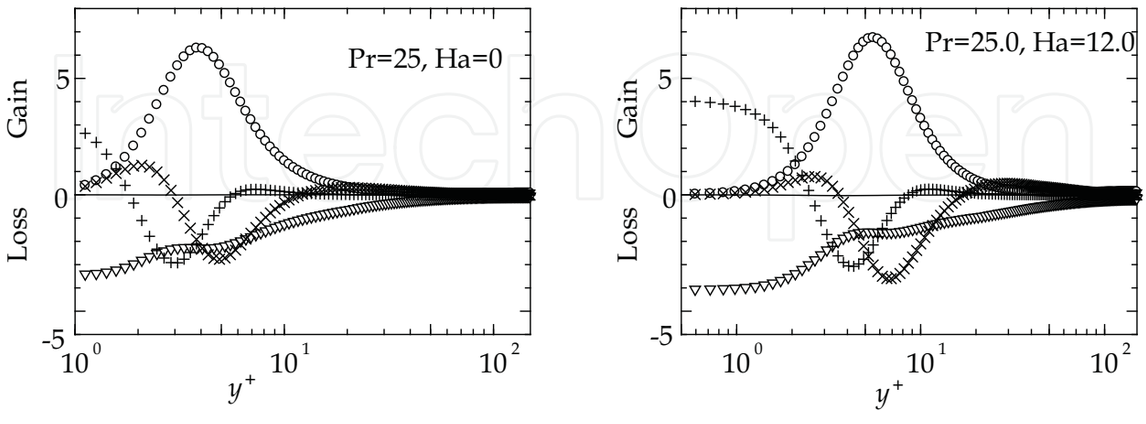

(a) Ha=0, Pr=25, (b) Ha=12, Pr=25,

Fig. 9. Budget of turbulent temperature energy

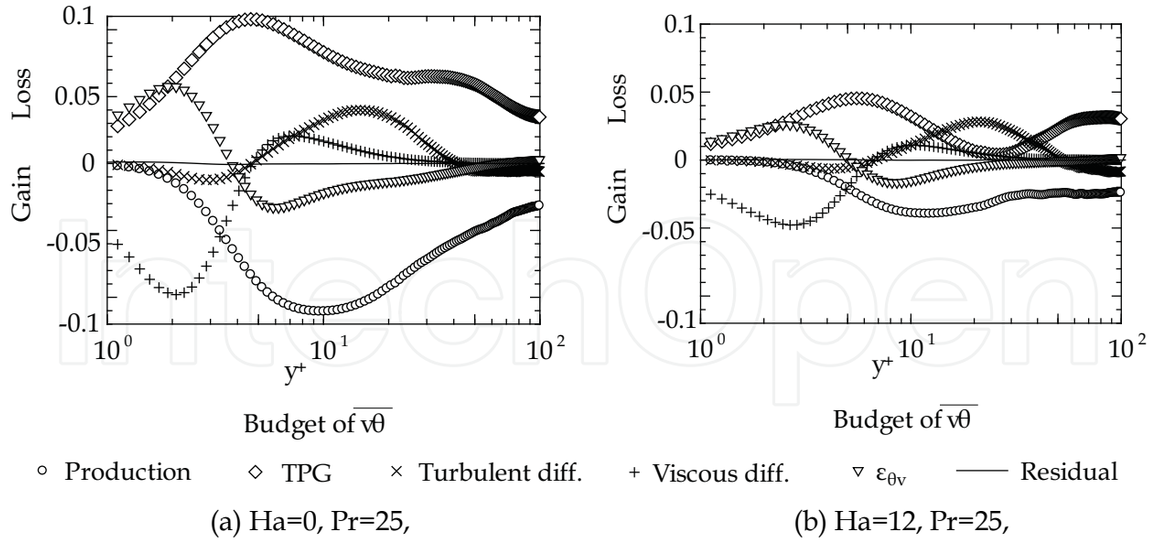

(a) Ha=0, Pr=25, (b) Ha=12, Pr=25,

Fig. 10. Budget of wall-normal turbulent heat flux

Figures 9 and 10 show the budget of turbulent temperature energy (K_θ) and wall-normal turbulent heat flux($v\theta$) for Pr=25, Ha=0 and 12. Transport equations (9) and (10) of turbulent temperature energy and wall-normal turbulent heat flux are expressed by

$$0 = \underbrace{-\overline{v\theta}\frac{\partial \Theta}{\partial y}}_{\text{Production}} \underbrace{-\frac{1}{2}\frac{\partial \overline{\theta\theta v}}{\partial y}}_{\text{Turbulent diff.}} + \underbrace{\alpha\frac{\partial^2 K_\theta}{\partial y^2}}_{\text{Viscous diff.}} - \underbrace{\alpha\overline{\left(\frac{\partial \theta}{\partial x_j}\right)^2}}_{\text{Dissipation:}\varepsilon_\theta}, \tag{9}$$

$$0 = \underbrace{-\overline{vv}\frac{\partial \Theta}{\partial y}}_{\text{Production}} \underbrace{-\frac{\partial \overline{\theta vv}}{\partial y}}_{\text{Turbulent diff.}} \underbrace{+\frac{\partial}{\partial y}\left(\nu\overline{\theta\frac{\partial v}{\partial y}} + \alpha\overline{v\frac{\partial \theta}{\partial y}}\right)}_{\text{Viscous diff.}} + \underbrace{\overline{p\frac{\partial \theta}{\partial y}} - \overline{\frac{\partial p\theta}{\partial y}}}_{\text{Temp.Press-Grad.}} \underbrace{-(\nu+\alpha)\overline{\frac{\partial \theta}{\partial x_j}\frac{\partial v}{\partial x_j}}}_{\text{Dissipation}}. \tag{10}$$

Here, over bar denotes quantities estimated by ensemble average. In Fig. 9-(a), around the thermal buffer region (y^+=5), both diffusion terms of turbulent and viscous exceeded dissipation (ε_θ) term. Predominance of the diffusion terms in the high-Pr fluids (Pr>10) was confirmed in the previous DNS (Schwertfirm &Manhart, 2007). In Ha=12, predominance of diffusion terms was observed more clearly as shown in Fig. 9-(b). As well as turbulent temperature energy, turbulent diffusion term in Fig. 10-(b) was dominant at y^+=15-30 in Ha=12, however, the predominance of viscous diffusion term was indistinct. Compared with no-MHD case in Fig. 9-(a), the damping of turbulent diffusion term was small but the others were suppressed by the MHD effects; effects of turbulent diffusion on the MHD heat transfer were relatively larger with increase of Ha. These indicate that a sensitive model of the turbulent diffusion would be required in the prediction of MHD heat transfer in high-Pr fluids.

Figure 11 shows the turbulent Prandtl number (Pr_T) profiles for Pr=5.7 and 25. Turbulent Prandtl number was defined as

$$\mathrm{Pr}_T = \overline{uv} / \overline{v\theta}\,. \tag{11}$$

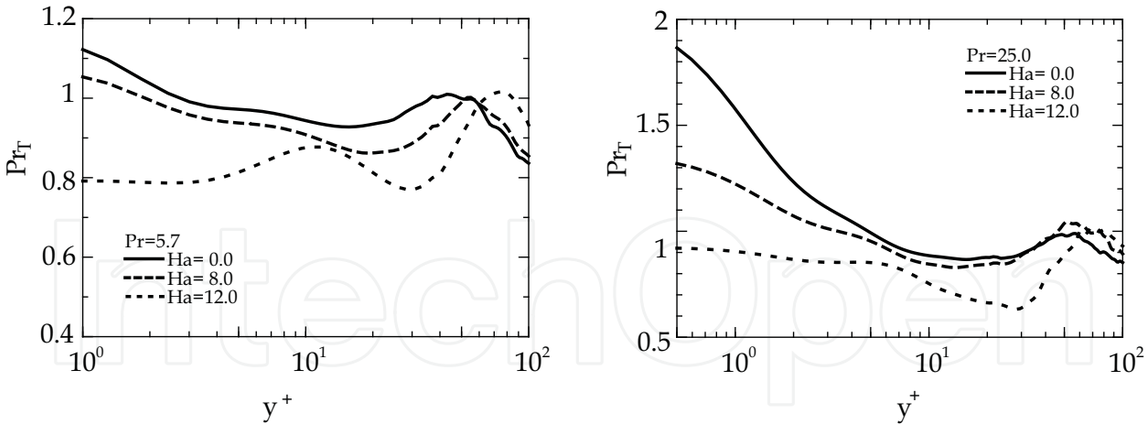

(a)Pr=5.7, (b) Pr=25,

Fig. 11. Turbulent Prandtl number profiles

Na & Hanratty, 2000 and Schwertfirm & Manhart, 2007 pointed out that turbulent Prandtl number close to the wall increases with increase of Pr. The turbulent Prandtl number profiles in the non-MHD case were good agreements with the results of Schwertfirm & Manhart, 2007, however, profiles in MHD case was decreased close to the wall for Pr=5.7 and 25 with increase of Ha. In Ha=12, the values of the turbulent Prandtl number in the vicinity of the wall fell into 1 for Pr=5.7 and 25. It was suggested that there was no MHD terms in balance of the heat transfer equation; turbulent effect on heat transfer might exceed that on momentum transfer as the limiting case of a turbulent-laminar transition status in Ha=12.

Figure 12 shows the time scale ratio for Pr=5.7 and 25. In non-MHD flow, time scale ratio had the weak peak at the buffer region for Pr=25 and 49 (Schwertfirm & Manhart, 2007 pointed out that). Time scale ratio profiles in MHD cases clearly had the peak in increase of Ha for Pr=5.7 and 25. At the buffer region, MHD effects on heat transfer might to be corresponded to the heat transfer in a higher-Pr fluid as shown in Figs. 9 and 12. However, these close to the wall might act on like a lower-Pr fluid as shown in Fig. 11.

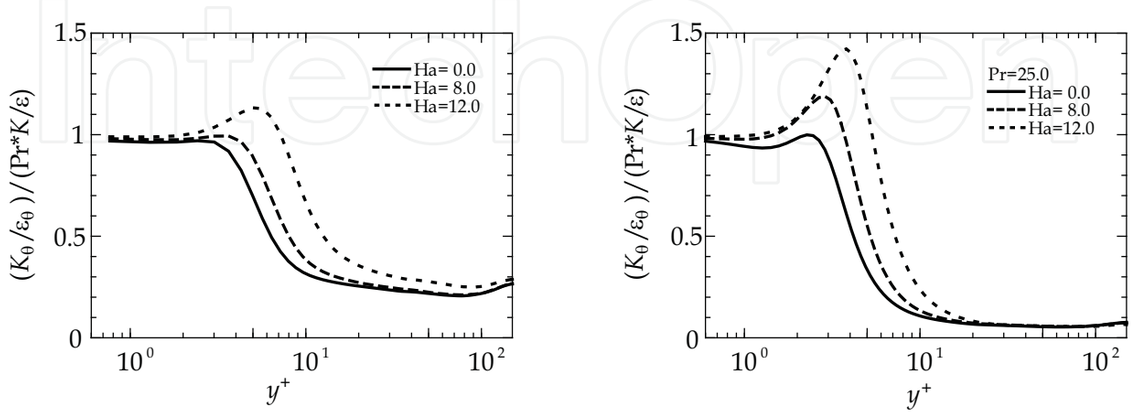

(a) Pr=5.7, (b) Pr=25,

Fig. 12. Time scale ratio profiles

Since both turbulent Prandtl number and time scale ratio were one of the dominant parameters in turbulent heat transfer modeling, change of profiles in increase of Ha might be caused the aggravation of the prediction accuracy.

7. Conclusion

In this study, direct numerical simulation of MHD turbulent channel flow for Prandtl number up to Pr=25 were performed. The adequacy of the present DNS data was verified by comparison with the DNS data fully-resolved the Batchelor length scale. As the results, the MHD turbulent heat transfer characteristics in Pr=25 were reported for the first time.
Maximum heat transfer degradation in the low-Pr fluid was no more than 5% of the non-MHD condition. On the other hands, heat transfer degradation in the high-Pr fluids (Pr=5.7 and 25) reached up to 30%. The similarity of heat transfer degradation in high-Pr MHD flows seemed be existed.
On the MHD heat transfer in high-Pr fluids, effects of turbulent diffusion were relatively larger. Turbulent Prandtl number and time scale ratio were considerably changed with increase of Ha.
The scaling of MHD heat transfer in high-Pr fluids was not understood yet. For the high-Ha and Re_τ condition (Ha>5, Re_τ>250), Boeck et al. 2007 reported the similarity of MHD mean velocity profiles on the parameter R(: Hartmann Reynolds number). To discuss the scaling of MHD heat transfer, we need DNS data of higher-Re and Ha conditions. In such cases, present DNS procedure by using a different resolution for flow and high-Pr temperature field will demonstrate a great advantage.

8. Acknowledgment

Present DNS were conducted by using the T2K open supercomputer at ACCMS and IIMC, Kyoto University. This study was supported by the Global COE program "Energy Science in the Age of Global Warming" and a Grant-in-aid for Young Scientists (B), KAKENHI (21760156) MEXT, Japan.

9. References

Batchelor, G.K., (1959), Small-scale variation of convected quantities like temperature in turbulent fluid. Part 1. General discussion and the case of small conductivity, *Journal of Fluid Mechanics,* Vol.5, pp.113–133.

Blum, E.YA., (1967), Effect of a magnetic field on heat transfer in the turbulent flow of conducting liquid, *High Temperature,*Vol. 5,pp. 68-74.

Boeck, T., Krasnov, D., and Zienicke, E., (2007), Numerical study of turbulent magnetohydrodynamic channel flow, *Journal of Fluid Mechanics*, Vol.572, pp.179-188.

Lee, D. & Choi, H., (2001), Magnetohydrodynamic turbulent flow in a channel at low magnetic Reynolds number, *Journal of Fluid Mechanics*, Vol.429, pp.367–394.

Na, Y. & T.J. Hanratty, T.J., (2000), Limiting behavior of turbulent scalar transport close to a wall, *International Journal of Heat and Mass Transfer*, Vol.43 , pp.1749-1758.

Patterson, S. & Orszag, S.A., (1971), Spectral calculations of isotropic turbulence: Efficient removal of aliasing interactions, *Physics of Fluids*, Vol.14, pp.2538-2541.

Reed, C.B. & Lykoudis, P.S., (1978), The effect of a transverse magnetic field on shear turbulence Journal of Fluid Mechanics, Vol.89, pp.147-171.

Sagara. A., Motojima, O., Watanabe, K., Imagawa, S., Yamanishi, H., Mitarai, O., Sato, T., Chikaraishi, H. and FFHR Group, Design and development of the Flibe blanket for helical-type fusion reactor FFHR, *Fusion Engineering and Design*, Vol.29, pp.51-56.

Satake, S., Kunugi, T., Takase, T., and Ose, Y., (2006), Direct numerical simulation of turbulent channel flow under a uniform magnetic field for large-scale structures at high Reynolds number, *Physics of Fluids*, Vol.18, 125106.

Schwertfirm, F. & Manhart, M., (2007), DNS of passive scalar transport in turbulent channel flow at high Schmidt numbers, *International Journal of Heat and Fluid Flow*, Vol.28, pp. 1204–1214.

Simomura Y., (1991), Large eddy simulation of magnetohydrodynamic turbulent channel flows under a uniform magnetic field, *Physics of Fluids* A 3, pp.3098-3106.

Yamamoto, Y.,Kunugi, T., Satake, S., and Smolentsev, S. (2008), DNS and k–ε model simulation of MHD turbulent channel flows with heat transfer, *Fusion Engineering and Design*, Vol.83, pp.1309-1312.

Yokomine, T., Takeuchi, J., Nakaharai, H., Satake, S., Kunugi, T., Morley, N.B., and M. A. Abdou, M.A., (2007), Experimental investigation of turbulent heat transfer of high Prandlt number fluid flow under strong magnetic field, *Fusion Science and Technology*, Vol.52, pp.625-629.

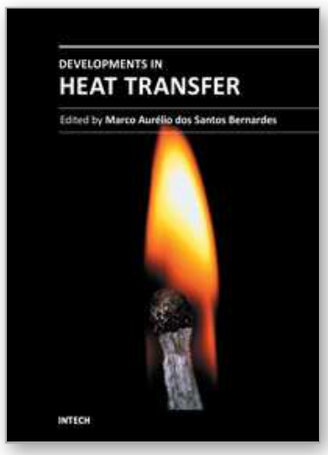

Developments in Heat Transfer

Edited by Dr. Marco Aurelio Dos Santos Bernardes

ISBN 978-953-307-569-3
Hard cover, 688 pages
Publisher InTech
Published online 15, September, 2011
Published in print edition September, 2011

This book comprises heat transfer fundamental concepts and modes (specifically conduction, convection and radiation), bioheat, entransy theory development, micro heat transfer, high temperature applications, turbulent shear flows, mass transfer, heat pipes, design optimization, medical therapies, fiber-optics, heat transfer in surfactant solutions, landmine detection, heat exchangers, radiant floor, packed bed thermal storage systems, inverse space marching method, heat transfer in short slot ducts, freezing an drying mechanisms, variable property effects in heat transfer, heat transfer in electronics and process industries, fission-track thermochronology, combustion, heat transfer in liquid metal flows, human comfort in underground mining, heat transfer on electrical discharge machining and mixing convection. The experimental and theoretical investigations, assessment and enhancement techniques illustrated here aspire to be useful for many researchers, scientists, engineers and graduate students.

InTech Europe
University Campus STeP Ri
Slavka Krautzeka 83/A
51000 Rijeka, Croatia
Phone: +385 (51) 770 447
Fax: +385 (51) 686 166
www.intechopen.com

InTech China
Unit 405, Office Block, Hotel Equatorial Shanghai
No.65, Yan An Road (West), Shanghai, 200040, China
中国上海市延安西路65号上海国际贵都大饭店办公楼405单元
Phone: +86-21-62489820
Fax: +86-21-62489821

IntechOpen